

BR1202–0725: An Extreme Multiple Merger at $z = 4.7$

P. Salomé¹, M. Guélin², D. Downes², P. Cox², S. Guilloteau³, A. Omont⁴, R. Gavazzi⁴, and R. Neri²

¹ LERMA, Observatoire de Paris, 61 av. de l’Observatoire 75014 Paris, France
e-mail: philippe.salome@obspm.fr

² Institut de Radio Astronomie Millimétrique (IRAM), Domaine Universitaire, 300 rue de la piscine, 38406 St Martin d’Hères, France

³ LAB, Observatoire de Bordeaux, 2 rue de l’Observatoire, BP 89, F-33270 Floirac, France

⁴ IAP, Institut d’Astrophysique de Paris, 98bis bd Arago, F-75014 Paris, France

Received 5 July 2012 / accepted 27 July 2012

ABSTRACT

The radio-quiet quasar BR1202–0725 ($z = 4.695$) is a remarkable source with a bright Northwest (NW) companion detected at submm and radio wavelengths but invisible in the optical. In the absence of amplification by gravitational lensing, BR1202–0725 would be the most luminous binary CO and far-IR source in the Universe. In this paper, we report observations with the IRAM Plateau de Bure interferometer of BR1202–0725 in the redshifted emission of the CO(5–4) and (7–6) lines, the [C I](³P₂–³P₁) line, a high angular resolution ($0.3'' \times 0.8''$) 1.3 mm map of the rest-frame, far-IR dust continuum, and a search for the CO(11–10) line. We compare these results with recent ALMA data in the [C II] line. Both the quasar host galaxy and its NW companion are spatially resolved in the molecular line emission and the dust continuum. The CO profile of the NW companion is very broad with a full width at half maximum of $\sim 1000 \pm 130 \text{ km s}^{-1}$, compared to $\sim 360 \pm 40 \text{ km s}^{-1}$ for the quasar host galaxy to the Southeast (SE). The difference in linewidths and center velocities, and the absence of any lens candidate or arc-like structure in the field, at any wavelength, show that the obscured NW galaxy and the SE quasar host galaxy cannot be lensed images of the same object. Instead, we find morphological and kinematic evidence for sub-structures in both the NW and SE sources. We interpret these results as strong indications that the BR1202–0725 complex is a group of young, interacting, and highly active starburst galaxies.

Key words. galaxies: high redshift – galaxies: individual: BR1202–0725 – techniques: interferometric – cosmology: observations

1. Introduction

Submillimeter observations of galaxies and quasars at high redshift provide invaluable clues about the activity of galaxy mergers leading to the formation of massive galaxies, and about the star-forming environment when the universe was young. These clues come from the redshifted emission of dust heated by newly-formed stars and from molecular and atomic lines from the dense molecular gas in which the stars are born. Since the early 1990s, massive galaxies at high redshift have been observed with ground-based millimeter and submm telescopes that can detect submm-selected starburst galaxies and host galaxies of optically selected quasars. These detections are pushing more and more into the epoch of re-ionization, and are currently out to $z = 7.1$; (Venemans et al. 2012).

One of the first high- z quasars that was detected and studied in detail in both thermal dust emission and in CO lines is the very luminous optically selected quasar BR1202–0725 at $z = 4.7$ (McMahon et al. 1994; Ohta et al. 1996; Omont et al. 1996; Benford et al. 1999; Carilli et al. 2002; Iono et al. 2006; Riechers et al. 2006). The source is remarkable because it has two distinct components: a Southeast (SE) source associated with the optically luminous quasar and an obscured Northwest (NW) source with no counterpart in the visible. The two submm dust continuum peaks, separated by $3.7''$ (linear distance

24 kpc),¹ have nearly identical CO redshifts of $z = 4.695$ (SE) and $z = 4.693$ (NW). The extreme infrared luminosity makes BR1202–0725 one of the brightest high- z sources ($L_{IR} = 3.7 \times 10^{14} L_{\odot}$, Leipski et al. 2010, confirming the original estimate by McMahon et al. 1994). The far-IR part of the luminosity is $L_{FIR} = 3.8 \times 10^{13} L_{\odot}$, with 1.2 and $2.6 \times 10^{13} L_{\odot}$ for the NW and SE galaxies (Iono et al. 2006). The estimated star-formation rate in each component is $\geq 1000 M_{\odot} \text{ yr}^{-1}$ and the combined molecular gas mass is $\sim 10^{11} M_{\odot}$ (Omont et al. 1996; Riechers et al. 2006).

The SE optical quasar host galaxy and the optically obscured NW source are both detected in the CO $J = 1 - 0$ through 7–6 rotational lines (Ohta et al. 1996; Omont et al. 1996; Carilli et al. 2002; Riechers et al. 2006) as well as in the [C II] emission line, the main cooling line in the interstellar medium (Iono et al. 2006; Wagg et al. 2012). At optical wavelengths, the SE component of BR1202–0725 appears as a quasar with at least two faint companion galaxies, seen in the optical (starlight) continuum (see our Fig. 6). The first of these optical continuum sources, found by Fontana et al. (1996) and Hu et al. (1996), is centered $2.6''$ northwest of the quasar, near to, but not coinciding with, the obscured NW submm source, and it appears to be part of a

¹ For linear sizes and luminosity distances we took the standard cosmology with $H_0 = 71 \text{ km s}^{-1} \text{ Mpc}^{-1}$, $\Omega_M = 0.27$, $\Omega_{\Lambda} = 0.73$ (Komatsu et al. 2011), and used the cosmological calculator by Wright (2006).

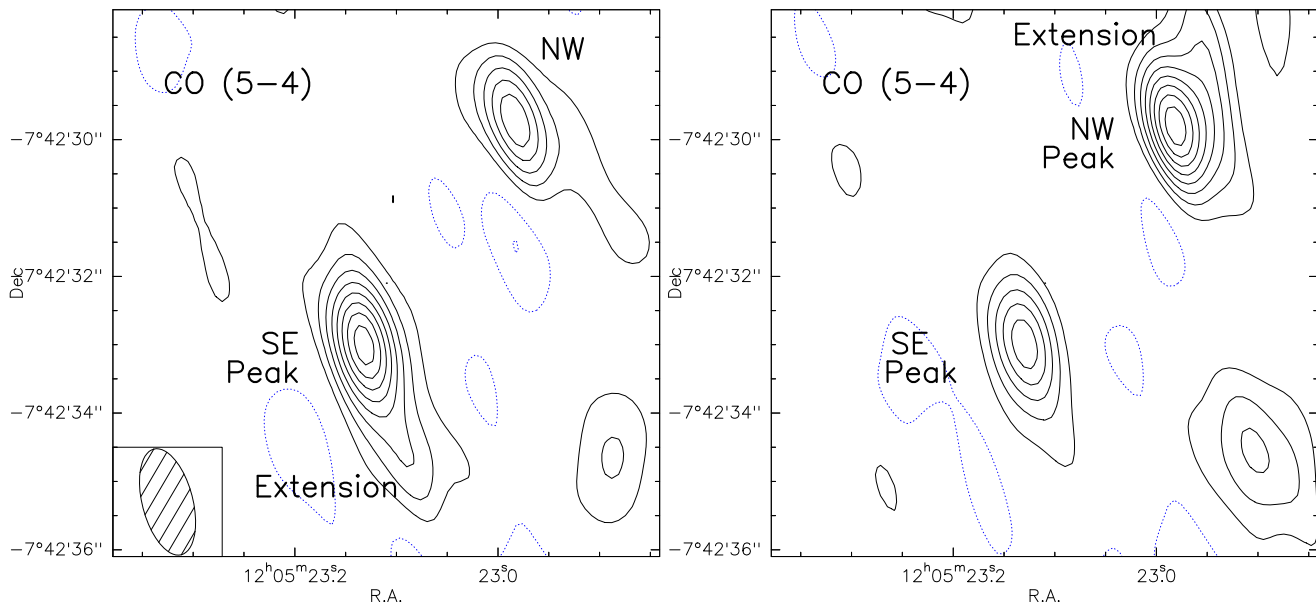


Fig. 1. Integrated CO(5–4) line maps, optimized to show total emission in the SE and NW galaxies separately. Source centroids and sizes are listed in Table 1. Both maps have natural weighting with a beam of $1.6'' \times 0.7''$ (PA 15° ; lower-left box in left panel). *Left:* CO(5–4) integrated over a 444 km s^{-1} -wide band, centered on the SE galaxy’s line center velocity. Contour steps are 0.24 mJy (1σ). The integrated CO(5–4) flux of the whole SE source, including the extension to the SW, is 1.6 Jy km s^{-1} . *Right:* CO(5–4) integrated over a 1067 km s^{-1} -wide band, centered on the NW galaxy’s line center velocity. Contour steps are 0.15 mJy (1σ). The integrated CO(5–4) flux of the whole NW source, including the extension to the northwest, over the 1067 km s^{-1} band, is 2.6 Jy km s^{-1} (see Table 2)

filament of optical starlight continuum emission extending over $4''$ away from the quasar. Part of this optical continuum source is prominent in Ly α emission at $z = 4.702$ (Hu et al. 1996; Petitjean et al. 1996; Ohyama et al. 2004). The second, fainter, optical starlight continuum source is also a Ly α emission galaxy, located $3''$ southwest of the quasar (Hu et al. 1997).

Up to now, detailed study of the profiles of the molecular and carbon fine structure lines in BR1202–0725 have been hampered by lack of sufficient bandwidth to cover the very broad molecular emission lines of the NW galaxy (Omont et al. 1996; Carilli et al. 2002). To remedy this situation, we present in this paper new wide-bandwidth spectral-line observations of CO and [C I] emission in BR1202–0725, along with high-angular resolution observations of the 1.3 mm thermal dust continuum. These new data from the Plateau de Bure interferometer (PdBI) are compared with submm data obtained with ALMA that trace the [C II] emission line and the 0.9 mm thermal dust continuum emission (Wagg et al. 2012). Our observations improve significantly on previous studies and shed new light on the kinematics of the SE and NW sources as well as on their structures. These data indicate that BR1202–0725 is a very complex group of merging starburst galaxies.

2. Observations and data reduction

The PdBI observed BR1202–0725 at 3 and 1.3 mm in February and March 2007 and at 2 mm in November 2011. In winter-spring 2007, the 6 antennas were in the extended A configuration with a longest baseline of 760 m . The receivers were successively tuned to 101.190 and 222.478 GHz , close to the redshifted frequencies of the CO(5–4) and CO(11–10) lines. Due to the low declination of the source,

the synthesized beam was elliptical with a FWHM of $1.6'' \times 0.7''$ (PA 15°) at 3 mm , and $0.85'' \times 0.26''$ (PA 15°) at 1.3 mm .

The November 2011 observations were made in the intermediate C configuration at 142.6 GHz , near the frequencies of CO(7–6) (redshifted to 141.637 GHz) and [C I]($^3\text{P}_2 - ^3\text{P}_1$) (redshifted to 142.110 GHz ; hereafter, we refer to this neutral carbon line simply as C I). The beam was $3.0'' \times 1.8''$ (PA 18°) at 2 mm .

The dual-polarization receivers operated in single side-band mode (LSB), with SSB receiver noise temperatures of $40\text{--}50 \text{ K}$. The observations were done in dry weather, with system noise temperatures of $\sim 140 \text{ K}$ at 2 and 3 mm and 180 K at 1.3 mm , after correction for atmospheric absorption and spillover losses. The IF bandwidth was 1 GHz in 2007 (3000 km s^{-1} at 3 mm , 1300 km s^{-1} at 1.3 mm) and 3.6 GHz in 2011 (7600 km s^{-1} at 2 mm). In the raw spectra, channel spacings were 2.5 MHz in 2007 and 2.0 MHz in 2011.

Amplitude and phase were calibrated every 20 minutes on 3C 273, whose flux was compared on each observing day to the continuum of the ultra-compact H II region around the star MWC 349 (taken to be 1.04 , 1.48 , and 1.67 Jy at 101 , 141 and 222 GHz , respectively).

Pointing and focus were checked every 40 minutes. The PdBI “seeing” parameter, which is not a limit on the radio resolution, but an indicator of the strength of the atmospheric phase fluctuations, was $0.33''$ to $0.49''$ at 3 and 2 mm and $0.23''$ to $0.26''$ at 1.3 mm . Short-term ($< 1 \text{ min}$) atmospheric phase fluctuations were corrected with the aid of 3-channel monitoring receivers centered on the 22 GHz atmospheric water line. Total on-source integration times, excluding flagged data, were 13.2 h at 3 mm , 5 h at 2 mm and 6 h at 1.3 mm . The data were calibrated with the GILDAS

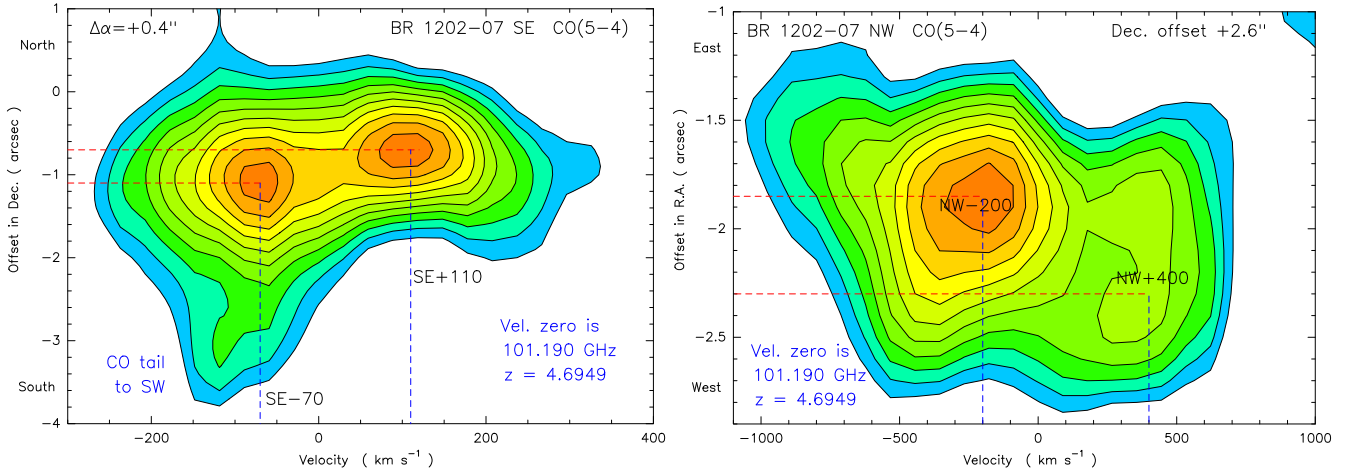


Fig. 4. Position-velocity diagrams of CO(5-4) in BR1202-0725. *Left:* Dec.-velocity cut through the SE source. The main line has two peaks, at -70 and $+110 \text{ km s}^{-1}$, separated by $+0.4''$ in dec. At negative velocities, a narrow-line CO tail extends $> 3''$ southwest. This tail to the SW is near, but does not coincide with, the weak SW continuum source found by Wagg et al. (2012). *Right:* R.A.-velocity cuts through the NW source. Note the large linewidth, and the weaker merger galaxy, which includes the strong line core near -200 km s^{-1} , and the weaker plateau, that may be another merger galaxy, at $+400 \text{ km s}^{-1}$, and $0.6''$ to the west or northwest. For both diagrams, velocity offsets are relative to 101.190 GHz ($z = 4.6949$), and contours start at 2σ and increase in steps of $1\text{-}\sigma$ (0.37 mJy/beam). The beam is $1.6'' \times 0.7''$ (PA 15°); position offsets are relative to the map phase center at RA 12:05:23.11, Dec $-07:42:32.10$ (J2000).

CLIC program; both polarizations were co-added and the maps were cleaned with the GILDAS MAPPING program.

3. Results

3.1. The 3-mm data: CO(5-4) line emission

Figure 1 shows two different CO(5-4) integrated intensity maps, made separately to best show the SE and NW galaxies, with a limited velocity range for the SE quasar host galaxy, and a much wider velocity range to show the total emission from the NW galaxy. These maps indicate that the CO in the NW galaxy is resolved to the north or northwest, in the direction of the beam minor axis (HPBW $0.7''$). They also indicate a probable extension or tail somewhat south or slightly southwest of the SE galaxy.

Figures 2, 3, and 5 show the CO(5-4) line data from the SE and NW galaxies in detail not previously seen. The most striking result is how dissimilar the spectra are. The CO profile of the SE galaxy, centered at redshift $z = 4.6952$, has a FWHM linewidth of $\Delta V = 360 \pm 40 \text{ km s}^{-1}$ (Table 2), comparable to those of other high- z quasar host galaxies detected in CO. In the local universe, such a linewidth is typical of massive spirals seen edge-on, and in the mid-range of linewidths for merging galaxies like some of the low- z ultraluminous infrared galaxies (ULIRGs), and the high- z submillimeter galaxies (SMGs; see, e.g., Fig. 6 of Bothwell et al. 2012).

In contrast, the NW galaxy has an extraordinarily broad profile with $\Delta V_{\text{FWHM}} \simeq 1000 \text{ km s}^{-1}$ and $\Delta V_{\text{FWZP}} \simeq 1700 \text{ km s}^{-1}$ (Fig. 4, right, and Table 2). These values exceed the CO linewidths normally observed in quasars or galaxies, with some notable exceptions like the 1500 km s^{-1} -wide CO line in the NGC 6240 merger (e.g., Feruglio et al. 2012), the high- z quasar-and-multiple-galaxy merger in SMM J02399-0136 (see Ivison et al. 2010 and references therein), and the $z = 3.8$ radio-galaxy merger in 4C41.17 (De Breuck et al. 2005). The main CO line peak in the

NW source is blue-shifted by -200 km s^{-1} relative to the CO centroid of the SE galaxy. This main CO peak dominates on the eastern side of the NW galaxy (Fig. 4, right). Toward the western side of the NW galaxy, there is a secondary spectral feature that is red-shifted by $+600 \text{ km s}^{-1}$ relative to the main CO peak in the NW galaxy. These two spectral features at -200 and $+400 \text{ km s}^{-1}$ suggest that the obscured NW submm object is in reality two merging galaxies, separated by about $0.6''$ (4.0 kpc).

The redshift of the $+400 \text{ km s}^{-1}$ component happens to be the same as the $z = 4.702$ redshift of the Ly α -1 galaxy between the NW and SE galaxies (Hu et al. 1996; Fig. 6). Like the CO lines from the NW merger, the Ly α line is also very broad with $\Delta V_{\text{FWZP}} \simeq 1500 \text{ km s}^{-1}$ and $\Delta V_{\text{FWHM}} \simeq 1100 \text{ km s}^{-1}$ (Ohyama et al. 2004). As in the CO in the NW and SE sources, there are also multiple velocity components within the main Ly α -1 galaxy, over a range of 500 km s^{-1} (Fontana et al. 1998; Ohyama et al. 2004). Hu et al. (1997) and Fontana et al. (1998) note that the C IV line, seen in the quasar, is absent in the Ly α -1 galaxy, so the Ly α is not reprocessed quasar radiation, but instead comes from star formation, at a rate of 15 to $54 M_{\odot} \text{ yr}^{-1}$. The broad Ly α linewidths may thus be due to superwind bubbles breaking out of the starburst and supernova regions in their parent galaxies. Because of these winds and because of optical depth effects, Ly α redshifts can give very biased measurements of the systemic redshifts of galaxies, so the true redshift of the Ly α -1 object may differ from its measured Ly α redshift by several hundred km s^{-1} .

As in the CO spectra (Fig. 2), the CO position-velocity diagram of the SE galaxy (Fig. 4, left) shows two main CO peaks separated by $0.4''$ to $0.5''$ in position, and by 180 km s^{-1} in velocity, that may indicate rotation of the molecular disk in the inner $r = 2 \text{ kpc}$ of the quasar host galaxy. There is also evidence of a weaker CO source or streamer extending $3''$ southwest of the SE galaxy. This tail is blueshifted by -100 km s^{-1} relative to zero velocity

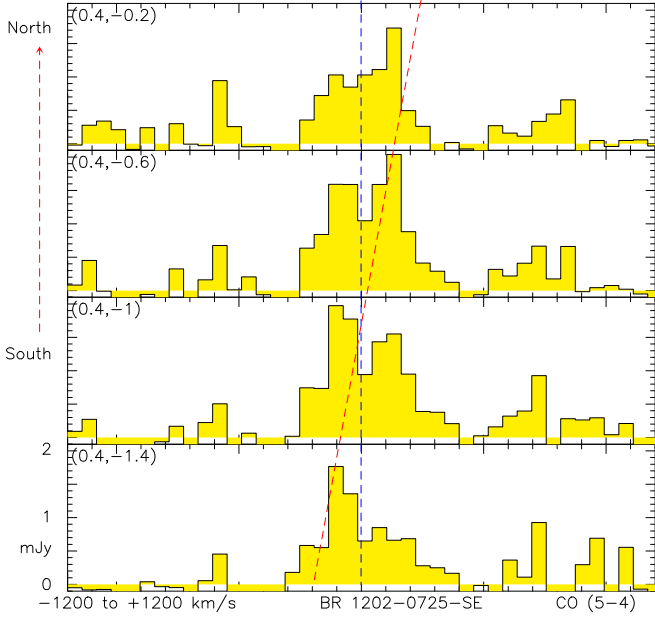


Fig. 2. CO(5-4) spectra across the SE galaxy, in steps of $0.4''$ in Dec. The tilted dashed line indicates how the two line components, at $+110 \text{ km s}^{-1}$ in the north, and -70 km s^{-1} in the south, cause the line centroid to shift relative to zero velocity (dashed vertical line through center of the spectra), in going from north to south (top to bottom). Position offsets in arcsec ($\Delta\alpha$, $\Delta\delta$, upper left of each panel), are relative to the map phase center at RA 12:05:23.11, Dec $-07:42:32.10$ (J2000). Velocity offsets (horizontal axes) run from -1200 to $+1200 \text{ km s}^{-1}$ relative to 101.190 GHz ($z = 4.6949$). The beam is $1.6'' \times 0.7''$ at PA 15° . Channel widths are 59.3 km s^{-1} ; $1\sigma = 0.48 \text{ mJy}$; the data are not convolved with any smoothing function.

in Fig. 4, left, and it has a relatively narrow linewidth (100 to 200 km s^{-1}). This weak CO tail to the southwest does not coincide, however, with the 0.9 mm continuum source reported by Waggoner et al. (2012). Nor do we see, at the position of their weak SW continuum source, any CO emission at velocities corresponding to the edge of the bandwidth used by Waggoner et al., where they had proposed a tentative detection of [C II].

The position-velocity diagram of the NW galaxy (Fig. 4, right) shows that the large linewidth in fact includes a strong core source centered at -200 km s^{-1} , and a weaker plateau, that may be another merger galaxy, at $+400 \text{ km s}^{-1}$. This second line component, also seen in the channel maps of Fig. 3, is $0.6''$ west or northwest of the main source, in direction of the extension seen on the 1.3 mm dust continuum map.

The 3-mm dust continuum is not visible in channel maps or in single-pixel spectra. From averaging the line-free channels on both ends of the spectra, we derive upper limits of 0.3 mJy (2σ) for both the SE and NW sources. Spectral baseline fits to the spatially-integrated spectra yield a spatially-integrated, 3-mm continuum flux density of $0.2 \pm 0.1 \text{ mJy}$ for the SE source, and are inconclusive for the NW source.

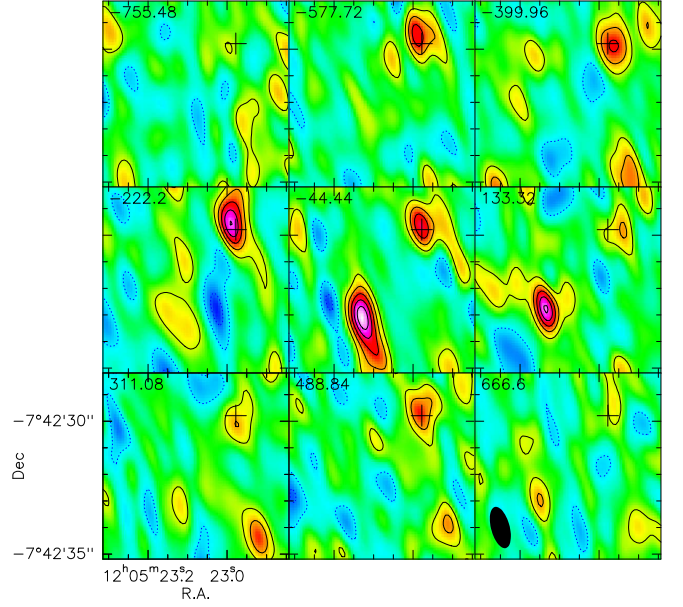


Fig. 3. CO(5-4) maps in 178 km s^{-1} -wide channels. The SE galaxy is strong at -44 and $+133 \text{ km s}^{-1}$ (middle row, center and right panels), while the NW galaxy (upper right of each panel) has a main maximum at -222 km s^{-1} (left column, middle panel), and a weaker plateau extending to positive velocities, notably in the panel at $+489 \text{ km s}^{-1}$ (lower row, middle panel). Contour steps are 0.34 mJy ; $1\sigma = 0.25 \text{ mJy}$. The cross in each box marks the position of the 1.3 mm continuum from the NE galaxy (Table 1). Velocity offsets (upper left corner of each box) are relative to 101.190 GHz ($z = 4.6949$). The beam is $1.6'' \times 0.7''$ (black ellipse in bottom right panel).

3.2. The 2-mm data: CO(7-6) and C I lines

Observations at 2 mm (142 GHz) show that the CO and [C I] lines are quite distinct in the SE source, where their spectral separation is larger than their linewidths. In the NW source however, due to their exceptionally broad widths, the CO(7-6) and C I lines are blended together (Fig. 5). For the NW source, because of this blending of the CO(7-6) and C I, and the two velocity components, we fixed the CO(7-6) linewidth to be the same as that of CO(5-4). The results for CO(7-6) and C I, from fitting a *single* Gaussian to each line are listed in Table 2. For the NW source, we show an alternative fit in Fig. 5, upper right and lower right, with two Gaussian velocity components in the NW source. In CO(5-4) (Fig. 5, upper right), this yields a main peak of $2.9 \pm 0.3 \text{ mJy}$, at $-260 \pm 40 \text{ km s}^{-1}$, with a linewidth of 737 km s^{-1} (FWHM). There is a secondary peak at $+440 \pm 64 \text{ km s}^{-1}$, with a width of 268 km s^{-1} . The two velocity components differ by $700 \pm 100 \text{ km s}^{-1}$, which agrees within the errors with the separation of the two velocity components in the channel maps of the NW source (Fig. 3), and in the position-velocity diagram (Fig. 4, right). The CO(7-6) line of the NW source (Fig. 5, lower right), is blended with the [C I] line, and a three- or four-component fit is needed. In the SE source, where the CO and [C I] lines are well separated (Fig. 5, lower left), the [C I] line has a width and center velocity consistent with those of the CO(7-6) and CO(5-4) lines (Table 2).

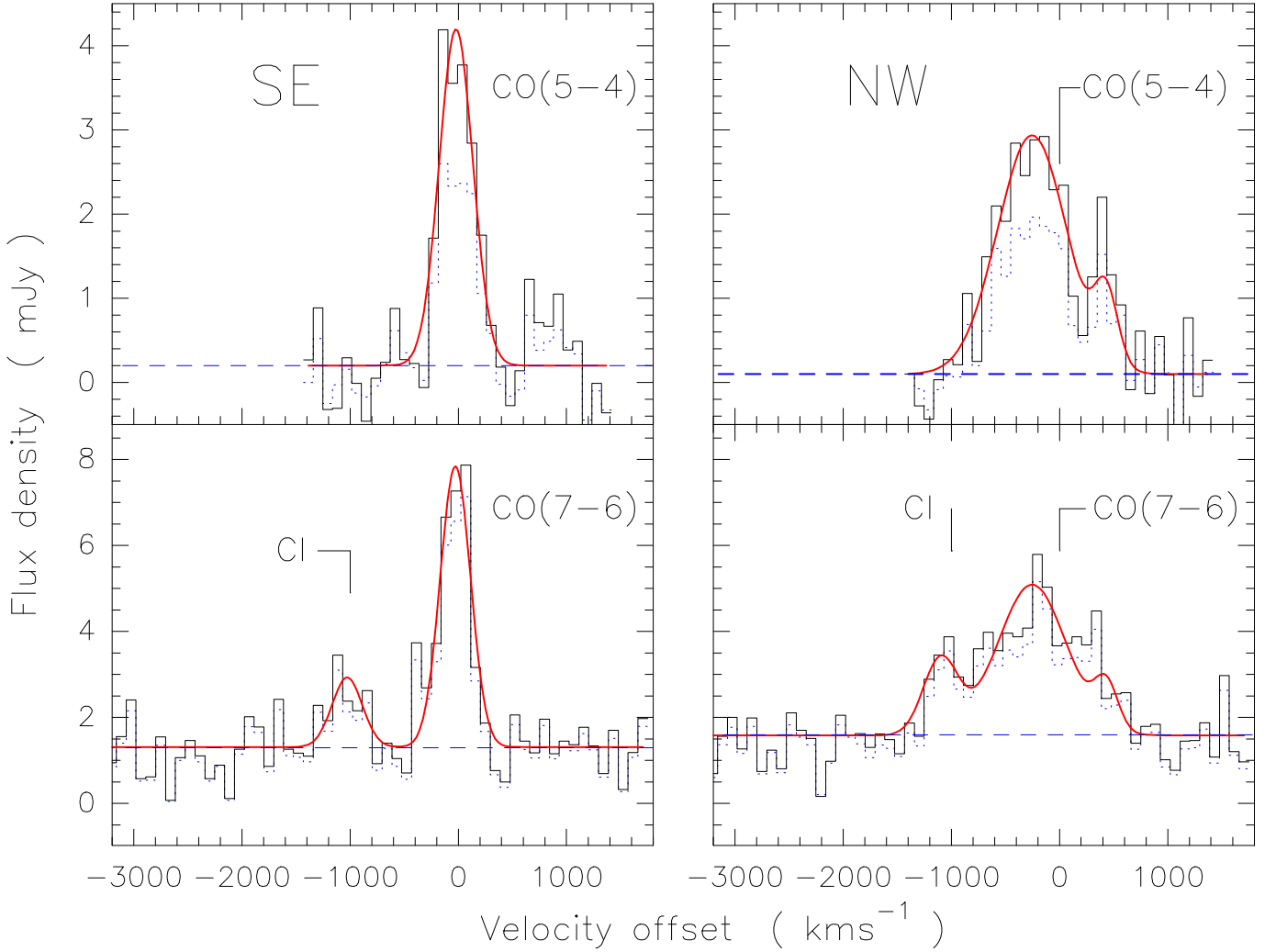


Fig. 5. CO(5–4), CO(7–6), and [CI]($^3\text{P}_2\text{--}^3\text{P}_1$) spectra of the SE and NW components of BR1202-0725. Histograms are spectra derived from fitting the interferometer visibilities by assuming elliptical Gaussian sources with sizes (FWHM) of $1.0'' \times 0.6''$ (SE) and $0.8'' \times 0.6''$ (NW). Solid curves show Gaussian spectral-line fits to the profiles, and dashed horizontal lines show continuum levels derived from these Gaussian spectral fits. The dotted histograms show alternative model-fit spectra for assumed point sources. The difference between model-point-source and model-extended-source spectra is more striking in CO(5–4) than in CO(7–6) because the larger beam in CO(7–6) more easily includes all the flux in each of the SE and NW sources. For the NW galaxy, two Gaussian velocity components are fit to the CO(5–4) and CO(7–6) lines, with a third Gaussian added to the CO(7–6) fit to include the CI line. Channel widths are 89 km s^{-1} and 91 km s^{-1} for CO(5–4) and (7–6) respectively, and velocity offsets (km s^{-1}) are relative to CO(5–4) and (7–6) redshifted to $z = 4.6952$.

For the 2 mm dust continuum, from both source maps and uv-fits, we obtain 2 mm continuum flux densities of 1.3 ± 0.2 and $1.6 \pm 0.2 \text{ mJy}$ for the SE and NW sources. In the $3.0'' \times 1.8''$ beam at 2 mm, the dust continuum sources are unresolved.

3.3. The 1.3 mm data: dust continuum and search for CO(11–10)

The high angular resolution of $0.26'' \times 0.85''$ ($1.8 \times 5.6 \text{ kpc}$ at $z = 4.7$) attained with the extended configuration of the PdBI at 1.3 mm enables us to study the thermal dust emission of BR1202-0725 in detail.

Figure 6 is a map of the 1.3 mm (222 GHz) continuum over the whole 1 GHz IF band. The band center was tuned to the redshifted frequency of CO(11–10). This line was not detected in the SE source, with a 3σ upper limit of

5 mJy/beam (Table 2). We see a 1.7σ hint of a line in the NW source, but more data are needed to confirm it.

The dust continuum source positions and uv-fit sizes are listed in Table 1. The SE and NW sources are well separated in the 1.3 mm continuum. The peak positions of the dust emission are close to the peaks of CO(5–4) reported in this paper, and also to the CO(2–1) peaks (Carilli et al. 2002) and the non-thermal cm-radio continuum peaks (Momjian et al. 2005).

The SE and NW sources are both resolved in the 1.3 mm continuum. Our model fits in the uv-plane yield equivalent circular Gaussian FWHM diameters of $0.5'' \pm 0.1''$ for the SE dust source, and $0.4'' \pm 0.1''$ for the NW source. More elaborate fits are not justified at present; a good rule of thumb is that one needs $S/N \geq 10$ to measure, e.g., major and minor axes and position angles. The spatially-

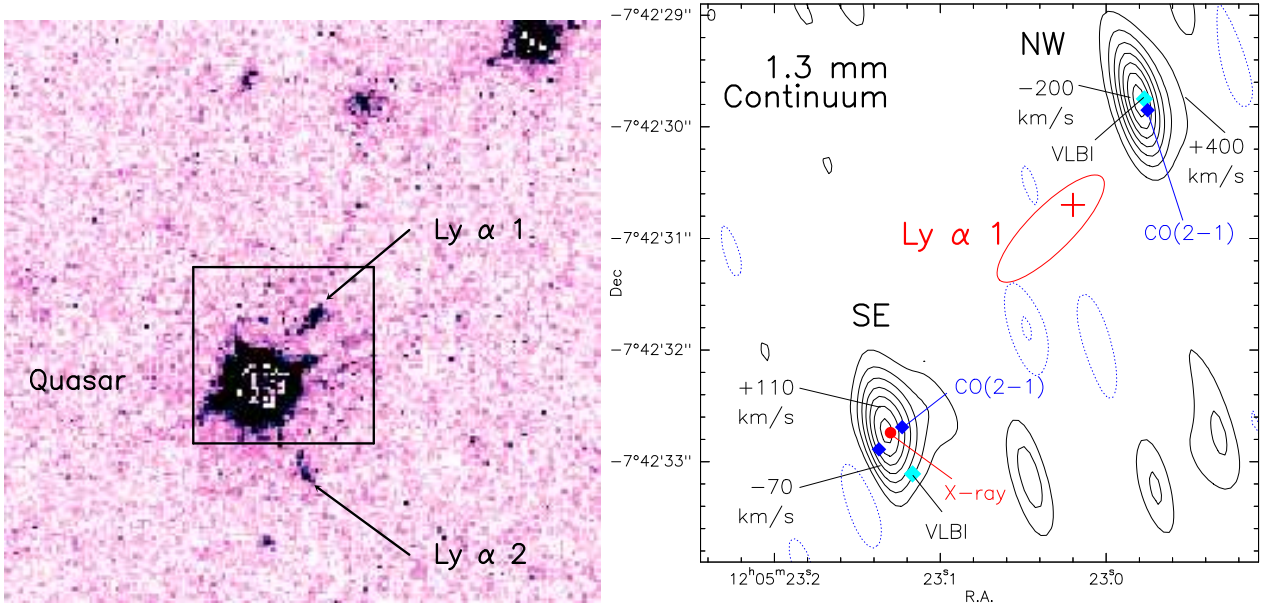


Fig. 6. *HST* image and 1.3 mm dust continuum map. *Left:* *HST* F814W image of the BR1202–0725 region (Hu et al. 1996) showing the quasar and the two galaxies with Ly- α redshifts measured by Hu et al. (1996; 1997). In this filter, the two Ly- α galaxies appear only in the starlight continuum, not the Ly- α line. The field is $16.4'' \times 16.4''$. The smaller box shows the $5'' \times 5''$ field of the 1.3 mm continuum map at the right. *Right:* Contours show the BR1202–0725 dust continuum at 1.3 mm in steps of 0.26 mJy/beam (1.5σ); negative contours are dashed, beam = $0.85'' \times 0.26''$. Next to the NW and SE galaxies separated by $3.7''$ are labels indicating the CO(5–4) velocity components discussed in the text, with offsets (km s^{-1}) relative to 101.190 GHz ($z = 4.6949$). The Ly- α -1 object, near the NW galaxy, is indicated by a red ellipse. The cross in the red ellipse marks the optical continuum peak, $2.6''$ from the quasar (Hu et al. 1996; 1997). The Ly- α peak is near the southern part of the ellipse, $2.3''$ from the quasar (Hu et al. 1996; Fontana et al. 1998; Ohyama et al. 2004). In the visible and near-IR, there is also a string of starlight continuum emission extending over $4''$ in the same direction, but displaced by $0.6''$ from the Ly- α -1 object (Hu et al. 1996; Fontana et al. 1998; Ohyama et al. 2004). In the SE galaxy (lower left) the central red dot indicates the X-ray source, coincident with the quasar (Evans et al. 2010). The blue dots show the VLA CO(2–1) peaks on either side of the quasar, and in the NW galaxy (Carilli et al. 2002). The light-blue diamonds show the extended non-thermal emission observed in VLBI at 1.4 GHz (Momjian et al. 2005). Source positions are listed in Table 1.

integrated flux densities are 5.1 ± 0.9 (SE) and $4.0 \pm 1.3 \text{ mJy}$ (NW).

The weaker dust source to the southwest of the quasar, reported by Wagg et al. (2012) at 340 GHz, is not seen in the 1.3 mm continuum map. Its 0.9 mm flux density of $1.9 \pm 0.3 \text{ mJy}$ implies a 1.3 mm flux $\leq 0.5 \text{ mJy}$, too low (2σ) to be seen on our current map.

4. Source properties

In the Appendix to this paper, we review evidence that the SE and NW sources in BR1202–0725 are not strongly gravitationally lensed. All source properties given in the following sections therefore have no correction factors for lensing.

4.1. The northwest source

The above results show that the NW source is resolved in both the CO(5–4) line and the 1.3 mm continuum, as seen in Figs. 3, 5, and 6. The CO line profiles clearly change, between positions separated by $0.5''$, on either side of the 1.3 mm continuum peak. The CO spectra and position-velocity diagrams across the NW source show that the sub-sources, or merging galaxies, have velocities that dif-

fer by 600 km s^{-1} , thereby explaining the unusually large linewidth of the overall CO profile.

4.2. The southeast source

As noted above, the CO(5–4) spectra of the SE galaxy show two line peaks separated by 180 km s^{-1} , and $0.4''$ to $0.5''$ (Figs. 2 and 4). These two *velocity* peaks are probably the same as the two *spatial* peaks of the SE galaxy, already seen by Carilli et al. (2002) who used a VLA beam of $0.3'' \times 0.2''$ to resolve the CO(2–1) emission into two components, oriented SE–NW and separated by $0.3''$. These two components are on either side of the quasar (Fig. 6), and may be in opposite sides of a disk rotating around the nucleus. In the 1.3 mm dust emission, the quasar host galaxy also appears to have a weaker extension $0.5''$ to the northwest (projected distance 3.3 kpc; Fig. 6).

From VLBI observations with the VLBA, the VLA, and the GBT, Momjian et al. (2005) claim that the SE 1.4 GHz nonthermal radio continuum peak is apparently $0.4''$ south of the quasar (Fig. 6, right, and Table 1), while the VLBI NW source coincides with the 1.3 mm NW dust peak. The SE displacement might be further evidence that the SE and NW sources have multiple components. The synchrotron emission sources seen in VLBI at 1.4 GHz are extended (diameters $0.3''$, or 2 kpc), with intrinsic brightness temper-

Table 1. Source positions and sizes.

Source	R.A. 12 ^h 05 ^m (J2000)	Dec. −07°42′ (J2000)	$\Delta\theta$ from SE-1.3mm continuum	Source size (FWHM)	Refs.
SE galaxy:					
SE 1.3 mm continuum	23.129 ^s ± 0.002 ^s	32.74″ ± 0.03″	0.0″	0.52″ ± 0.06″	1
Chandra X-ray catalog	23.130 ^s ± 0.02 ^s	32.74″ ± 0.3″	0.0″	—	2
CO(2–1) SE (nw subpeak)	23.122 ^s ± 0.003 ^s	32.71″ ± 0.05″	0.1″	≤ 0.25″	3
CO(2–1) SE (se subpeak)	23.134 ^s ± 0.003 ^s	32.92″ ± 0.05″	0.1″	≤ 0.25″	3
CO(5–4) SE centroid	23.130 ^s ± 0.002 ^s	32.94″ ± 0.06″	0.2″	0.5″ ± 0.1″	1
1.4 GHz nonthermal SE source	23.1167 ^s ± 0.04 ^s	33.109″ ± 0.3″	0.42″	0.30″ × 0.17″, 130°	4
NW galaxy:					
NW 1.3 mm continuum	22.978 ^s ± 0.002 ^s	29.79″ ± 0.03″	3.7″	0.26″ ± 0.04″	1
CO(2–1) NW	22.975 ^s ± 0.003 ^s	29.85″ ± 0.05″	3.7″	≥ 0.5″	3
CO(5–4) NW centroid	22.971 ^s ± 0.004 ^s	29.67″ ± 0.06″	3.8″	0.7″ ± 0.1″	1
1.4 GHz nonthermal NW source	22.977 ^s ± 0.04 ^s	29.750″ ± 0.3″	3.7″	0.29″ × 0.17″, 115°	4

Position refs.: (1) This paper: our positions and sizes are from uv-fits to circular Gaussian models, and our absolute astrometric accuracy is 0.1″;

(2) Evans et al. (2010); (3) Carilli et al. (2002); (4) Momjian et al. (2005).

atures of 2×10^4 K at their 8 GHz rest frequency. With a typical nonthermal T_b spectral index of -2.7 , they would have a rest-frame 1.4 GHz T_b of 2×10^6 K — about 500 times higher than in the central hundred parsecs of M82. This non-thermal radio brightness is comparable with those of compact starbursts in ULIRGs. The BR1202-0725 nonthermal radio sources are therefore also likely to be the products of extreme starbursts rather than active galactic nuclei (AGNs; Momjian et al. 2005).

4.3. Molecular gas properties

We estimated the molecular H_2 gas densities and kinetic temperatures in the NW and SE sources by comparing the observed CO luminosities with single-component model brightness temperatures in the RADEX 1-D escape probability program (Van der Tak et al. 2007). The data on CO(5–4), (7–6), and (11–10) are from this paper; the CO(2–1) intensities were derived from Carilli et al. (2002) (see Table 2). These are the only data sets that have both good sensitivity and clear separation of the SE and NW sources, and they thus provide the first opportunity to model the CO Spectral Energy Distribution (CO-SED) for the NW and SE sources separately (Fig. 7).

We have no data from high density tracers like HCN and not yet enough spatial resolution for CO lines above CO(5–4). The kinetic temperatures and H_2 densities are therefore poorly defined. There are two main constraints: (1) in both sources, the CO(5–4) and (7–6) line luminosities, L' , are nearly equal, and (2) in both sources, the CO(11–10) is very weak, and not detected, at least in the SE source, with a luminosity at least four to five times lower than the CO(5–4) luminosity (Table 2).

If the gas temperature is in the range 40 to 50 K, i.e., typical of gas temperatures in ULIRGs, and close to the dust temperatures derived below, these constraints imply that the optical depths of the CO lines are high, at least up to the CO(7–6) line. Thanks to the collisional excitation and the resonant radiative trapping, the populations

of levels $J < 8$ are then nearly thermalized ($T_{ex} \simeq T_k$), so that line brightness temperatures and luminosities L' remain constant. In higher rotational transitions, the line opacity decreases, and unless the H_2 density is unrealistically large ($> 10^6$ cm $^{-3}$), this leads to a steep decrease in line brightness temperature.

The key is the high optical depth in CO. The practical consequence for the BR1202-0725 sources is that in flux units, because of the weighting by ν^2 , the CO spectral-line energy distribution peaks around $J=8$ (Fig. 7).

For comparison with escape probability models, we assumed the CO abundance was $X_{CO} = 10^{-4}$, and we took the microturbulence to be $1 \text{ km s}^{-1} \text{ pc}^{-1}$, both of which are standard values often assumed for Galactic molecular clouds. We took the background radiation field to be the cosmic background, at a temperature of 15.6 K at $z=4.7$, and we assumed gas kinetic temperatures of 43 K, the value estimated from the continuum dust spectra. In this zone of kinetic temperature, escape probability models can reproduce the two constraints listed above for a nearly constant value of the product

$$n(H_2) \cdot \frac{N_{CO}}{\Delta v} = 1.2 \times 10^{23}, \quad (1)$$

where $n(H_2)$ is the H_2 density in cm $^{-3}$, and $N_{CO}/\Delta v$ is the CO column density, in cm $^{-2}$ per microturbulent linewidth Δv , in km s $^{-1}$.

Realistic, optically-thick combinations would thus be $n(H_2) = 2 \times 10^3$ cm $^{-3}$, and $N_{CO}/\Delta v = 6 \times 10^{19}$ cm $^{-2}$ (km s $^{-1}$) $^{-1}$, for both the SE and NW galaxies. The upper range would be $n(H_2) = 2 \times 10^4$ cm $^{-3}$, and $N_{CO}/\Delta v = 6 \times 10^{18}$ cm $^{-2}$ (km s $^{-1}$) $^{-1}$. A solution in this range would be consistent with the gas mass (see next section), and with the dust becoming optically thick near rest-frame 100 μm .

Lowering the CO abundance, or CO column density, or increasing the microturbulence would require higher densities of molecular hydrogen to fit all the data. These simple models predict a CO(5–4) brightness temperature of 25 K, i.e., close to the Rayleigh-Jeans equivalent of ($T_{ex} - T_{bg}$),

Table 2. Observed parameters of CO and atomic lines, and continuum fluxes.

Line and Source	Reference frequency GHz	Line peak ^a mJy	Line width ^a km s ⁻¹	Center velocity ^a km s ⁻¹	Integrated intensity ^b Jy km s ⁻¹	Line luminosity L' ^b 10 ¹⁰ K km s ⁻¹ pc ²	Continuum S_{cont} ^b mJy
CO(5–4)	101.185						
SE	—	4.1 ± 0.4	363 ± 37	-17 ± 17	1.6 ± 0.2	5.3 ± 0.8	0.2 ± 0.1
NW-main peak	—	2.9 ± 0.3	737 ± 90	-260 ± 40	2.3 ± 0.3	7.8 ± 1.2	< 0.3 (2σ)
NW-extension	—	0.9 ± 0.1	268 ± 50	$+440 \pm 64$	0.3 ± 0.1	0.9 ± 0.1	< 0.3 (2σ)
NW-total	—	—	—	—	2.6 ± 0.4	8.7 ± 0.1	< 0.3 (2σ)
CO(7–6)	141.637						
SE	—	6.7 ± 0.5	316 ± 40	-27 ± 13	2.3 ± 0.2	3.9 ± 0.4	1.3 ± 0.1
NW-main peak	—	3.6 ± 0.3	737 ± 90	-260	2.8 ± 0.3	4.8 ± 0.5	1.6 ± 0.1
NW-extension	—	1.2 ± 0.1	268 ± 50	$+440$	0.3 ± 0.1	0.9 ± 0.1	—
NW-total	—	—	—	—	3.1 ± 0.4	5.7 ± 0.6	1.6 ± 0.1
[C I](³P₂–³P₁)	142.109						
SE	—	1.7 ± 0.4	316	—	0.6 ± 0.2	0.9 ± 0.3	1.3 ± 0.1
NW	—	1.8 ± 0.3	368	—	0.7 ± 0.2	1.2 ± 0.4	1.6 ± 0.1
CO(11–10)	222.471						
SE	—	< 3.8 (2σ)	—	—	< 1.4 (2σ)	< 1.0 (2σ)	5.1 ± 0.9
NW	—	2.7 ± 1.7	—	—	2.9 ± 1.8	2.0 ± 1.2	4.0 ± 1.3
[C II]^c	334.96						
SE	—	27	328 ± 6	210	9.6 ± 1.5	3.0 ± 0.5	18 ± 3
NW	—	20	722 ± 12	60	14.7 ± 2.2	4.6 ± 0.7	19 ± 3
CO(2–1)	40.479						
SE	—	0.77 ± 0.1	—	—	0.23 ± 0.04	4.8 ± 1.0	< 0.16 (2σ)
NW ^d	—	0.66 ± 0.1	—	—	0.39 ± 0.08	8.1 ± 2.0	< 0.16 (2σ)

^a Line peak fluxes, FWHMs, and velocities at the source peaks, from single-Gaussian spectral fits in velocity.

^b Line intensities, L' , and S_{cont} are over $1.0'' \times 0.6''$ (SE) and $0.8'' \times 0.6''$ (NW); line luminosity L' from formula of Solomon et al. (1992).

^c [C II] data from Wagg et al. (2012).

^d CO(2–1) flux in NW source (Carilli et al. 2002) corrected for limited VLA bandwidth by multiplying by 1.5, the ratio of the CO(5–4) flux in the full line width, to that in the limited VLA band of -525 to 175 km s⁻¹.

the difference between the (Planck) excitation temperature and the cosmic background at the CO(5–4) rest frequency of 576 GHz. Figures 2 and 3 show that the peak CO(5–4) brightnesses are 2.0 and 1.5 mJy beam⁻¹ in the SE and NW galaxies respectively. At 101.2 GHz, the $1.6'' \times 0.7''$ beam yields 107 K Jy⁻¹, so in our beam, the observed peak brightness temperatures, corrected for $(1+z)$, are 1.2 and 0.9 K for the SE and NW galaxies. If the source sizes at the velocities of the CO spectral peaks are about $0.3''$, or about the measured sizes of the dust sources, or about half the size of the entire line sources integrated over all velocities, then the true, deconvolved CO(5–4) peak line brightness temperatures, corrected for beam dilution, are 17 and 13 K for the SE and NW galaxies, or within a factor two of the predicted brightness temperature of 25 K from the simplest radiative transfer model.

More complicated fits with multi-temperature and multi-density components would change these results, and meaningful values for T_k and $n(\text{H}_2)$ are hard to derive because of the parameter degeneracy. In spite of the uncertainties, we can conclude, in agreement with previous studies, that much of the molecular gas in both of the BR1202–0725 sources is dense and warm.

4.4. Gas mass and dynamical mass

We use the CO(1–0) line luminosity-to-(H₂+He)-gas mass conversion factor derived for the center of ULIRGs by Downes & Solomon (1998),

$$M_{\text{gas}}/L'_{\text{CO}1-0} = 0.8 M_{\odot} (\text{K km s}^{-1} \text{ pc}^2)^{-1} \quad (2)$$

to estimate the gas mass in the SE and NW galaxies.

We took the CO(1–0) luminosities to be equal to the CO(5–4) luminosities. There are two reasons to do this, observational and theoretical. Firstly, direct measurements show that the CO(5–4) luminosities are equal to the CO(2–1) luminosities (Table 2), which means that in the CO levels $J < 5$, the CO is optically thick and thermalized. Furthermore, the total (SE+NW) CO(5–4) luminosity of 1.3×10^{11} K km s⁻¹ pc² is not only the same as the total (SE+NW) CO(2–1) luminosity, but also the same within the errors as the total (SE+NW) CO(1–0) luminosity of 1.0×10^{11} K km s⁻¹ pc² obtained in the single-dish CO(1–0) observations by Riechers et al. (2006).

Secondly, at $z = 4.7$, the CO(1–0) excitation temperature and the gas kinetic temperature have to be warmer than the cosmic microwave background temperature of nearly 16 K for CO(1–0) to be in emission; otherwise CO(1–0) would be in absorption (up to now never observed in

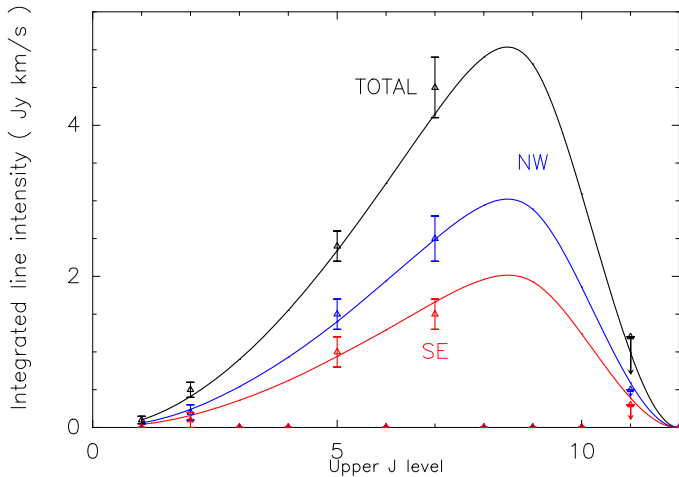


Fig. 7. CO line peak flux densities vs. upper J level, for the SE (red lower curve) and NW (blue middle curve) galaxies of BR1202-0725. The top black curve shows their sum. CO(1–0) data are from Riechers et al. (2006); CO(2–1) from Carilli et al. (2002); all other data are from this paper. The curves correspond to the radiative-transfer models described in the text.

high- z sources), or have too low a contrast relative to the CMB to be detectable. In standard radiative transfer models for gas warmer than 20 K (in order to have CO(1–0) in emission), and with $n(\text{H}_2)$ greater than 500 cm^{-3} (to collisionally excite the CO), and with high enough N_{CO} (to make the CO opaque enough to be detectable), the brightness temperatures of CO(1–0) and CO(5–4) are the same. Hence at $z = 4.7$, at every place you detect CO(1–0), you will also detect CO(5–4) — with the same brightness. At $z = 4.7$, there is no extra “reservoir” of “cold” CO(1–0) that is currently detectable.

We therefore take the CO(1–0) luminosities equal to the CO(5–4) luminosities, namely $L' = (5.3 \text{ and } 7.8) \times 10^{10} \text{ K km s}^{-1} \text{ pc}^2$ for the SE and NW-main galaxies (Table 2), and thus derive $M_{\text{gas}} = (4.2 \text{ and } 6.2) \times 10^{10} M_{\odot}$ for SE and NW-main, respectively. For both galaxies, the CO luminosities and consequently, the gas masses, are larger than in local ULIRGs, and comparable to the mean values of the SMGs listed by Bothwell et al. (2012; see their Fig. 6). For BR1202-07, these high CO luminosities and gas masses are probably partly the result of the sources’ multiplicity.

Similarly, we can estimate the gas mass from the CI line, using the formulae of Weiss et al. (2003; 2005). Assuming the same excitation temperature as for CO, and a [CI/H₂] ratio of 3×10^{-5} by number (1.8×10^{-4} by mass), we derive gas masses of $(5.3 \text{ and } 6.7) \times 10^{10} M_{\odot}$ for the SE and NW-main galaxies, i.e., similar to the gas mass estimated from CO.

Lower limits to the dynamical masses can be estimated from the CO linewidths and the source sizes. For the inner parts of the sources (the sizes derived from the fits to the 1.3 mm continuum), we derive the dynamical masses of the SE and NW sources from

$$M_{\text{dyn}}(\leq R) = \frac{R \cdot V^2}{G} = 232 R \cdot V_{\text{rot}}^2 \quad (3)$$

where $1/G = 232$, when M_{dyn} is in M_{\odot} , R is in pc, and V_{rot} is in km s^{-1} (e.g., Solomon et al. 1987). In principle, the rotation velocity could be estimated from the observed linewidths ΔV_{FWHM} , which would at face value imply true rotation velocities of 360 and 970 km s^{-1} for the SE and NW sources. In practice, these objects are dominated by the gas mass rather than the stellar mass, and have thick disks, with chaotic, merger-driven, and probably non-circular gas orbits. Above all, the turbulent velocities in the molecular gas in advanced mergers and ULIRGs are very large, of the order of 100 to 150 km s^{-1} (Downes & Solomon 1998). Furthermore, the position-velocity diagram for the NW source (Fig. 4b) indicates that the NW CO source is multiple; the strong core of the CO line, with a width of $\sim 400 \text{ km s}^{-1}$ corresponds to the main NW galaxy and its 1.3 mm dust continuum, while the plateau in the CO emission to higher velocities may be the other galaxy in the NW merger, possibly the weaker satellite extension seen on the dust continuum map. If we take the 400 km s^{-1} CO linewidth associated with the $0.6''$ -diameter CO source, and correct downward for turbulent broadening, the true rotation velocity would be 300 to 350 km s^{-1} , comparable to a rotation velocity we might deduce for the SE galaxy. Hence the dynamical mass within a radius of 2 kpc ($\sim 0.3''$) in both galaxies would be of the order of $6 \times 10^{10} M_{\odot}$ for each of the SE and NW sources.

Comparison of these dynamical masses of $6 \times 10^{10} M_{\odot}$ with the gas masses of 4.2×10^{10} and $6.2 \times 10^{10} M_{\odot}$ indicates that in the inner parts of the SE and NW galaxies, most of the mass is in the form of molecular gas. It also means that it would be difficult in these galaxies to have a CO-to-H₂ mass conversion factor much larger than the value for ULIRGs; otherwise, the gas mass within the central $r = 2 \text{ kpc}$ would greatly exceed the dynamical mass.

4.5. Dust mass and infrared luminosity

The dust properties in BR1202-0725 have been discussed by Benford et al. (1999), Iono et al. (2006), Leipski et al. (2010) and Wagg et al. (2012). To these studies, the results in this paper now add new measurements at 1.35, 2, and 3 mm that update previous data from Omont et al. (1996) and Guilloteau (2001). For the NW and SE sources, the updated dust continuum fluxes are given in Table 2.

For an estimate of the dust mass, we assumed a source size of $0.5''$, for consistency with the uv-fit sizes derived from the observed 1.3 mm continuum sources, and a dust mass opacity coefficient of $\kappa(\nu_r) = 10 \cdot \nu_r^{\beta}$, where ν_r is the rest-frame (emitted) frequency in THz, κ is in $\text{cm}^{-2} \text{ gm}^{-1}$ of dust, and we took the index $\beta = 2$. This absorption coefficient agrees with extensive literature estimates for very dense molecular clouds with coagulated dust particles (e.g., Krügel & Siebenmorgen 1994; Ossenkopf & Henning 1994). Because our observing frequencies correspond to rest frequencies well into the far-IR, where the large quantity of dust starts to become opaque, it is important in these estimates of dust mass not to use the standard formula for optically-thin dust. Instead, one must do a proper fit of the dust source function minus the background source function (see eq.(1) of Weiss et al. 2007). Because at $z = 4.7$, the cosmic background temperature is 16 K, it is important to subtract the background from the dust source function, as it reduces the source-to-background contrast for the ob-

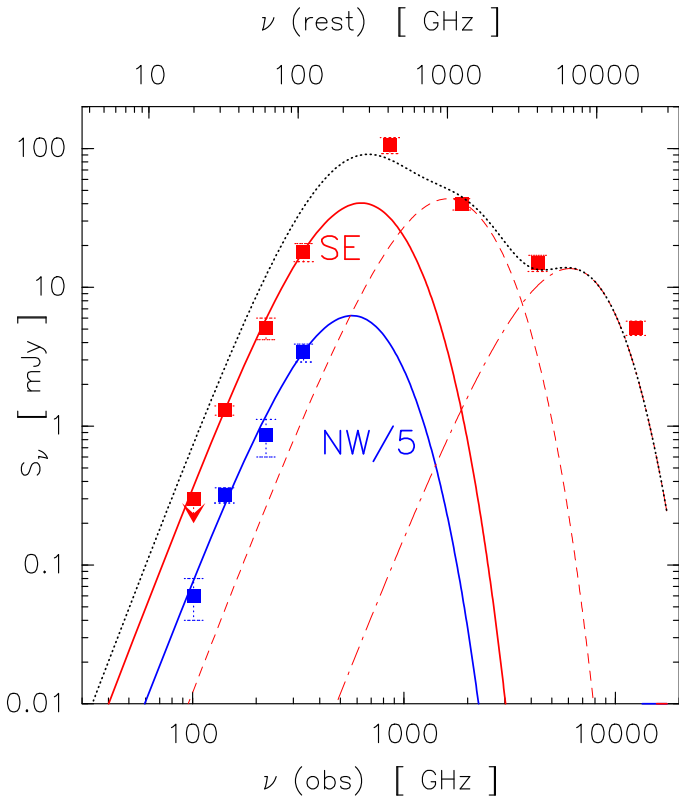


Fig. 8. Dust continuum spectra for NE and SW galaxies in BR1202-0725. Flux densities from 100 to 340 GHz are from the mm/submm interferometer data, as these are the only observations that spatially separate the NW and SE galaxies in the cool dust continuum: 101, 142, and 222 GHz from this paper, 340 GHz from Wagg et al. (2012). Because the mm/submm dust continuum fluxes of the two galaxies are nearly the same, we plot the NW galaxy fluxes (blue lower curve) divided by five, for better readability. Data points at 350, 160, 70, and $24 \mu\text{m}$ are from Benford et al. (1999), Leipski et al. (2010), and Hines et al. (2006). The red curves show model dust components for the SE galaxy: a starburst-heated 50 K component and two quasar-heated warm (130 K) and hot (410 K) dust components. The uppermost dotted curve is the total emission.

served dust flux. Applying this method to the mm/submm interferometric data only, which are the only observations that spatially separate the dust continuum of the NW and SE galaxies, we can fit the observed data (Fig. 8) with a dust temperatures of 40 to 50 K in both sources. The luminosities of these “cool”, “starburst” dust components alone, from integrating over the range 20 to $1000 \mu\text{m}$ (rest-frame) under the modified Planck functions in our models, are $6.3 \times 10^{12} L_{\odot}$ (SE) and $1.2 \times 10^{13} L_{\odot}$ (NW), comparable with values derived in previous studies. These values yield dust masses of $\sim 4 \times 10^8 M_{\odot}$ in both the NW and SE sources.

The flux densities from 350 to $24 \mu\text{m}$ (rest-frame 60 to $4.2 \mu\text{m}$), follow the usual quasar-template monotonic decrease (a flat curve when plotted as νS_{ν}), due to quasar-heated dust from a continuous distribution of dust layers of increasing density and decreasing mass and size as one moves inward toward the quasar. Following the model of Weiss et al. (2003) for the Cloverleaf quasar, we approx-

imate this continuous distribution with just two components, a “warm” (130 K) layer of size $0.11''$, and a “hot” (410 K) layer of size $0.014''$. This approximation (Fig. 8) shows that nearly all the rest-frame mid-IR and near-IR flux comes only from the SE galaxy (the quasar); the mid-to-near-IR contribution of the NW galaxy is negligible. The $350 \mu\text{m}$ flux measured by Benford et al. (1999; rest frame $60 \mu\text{m}$), comprises not only the fluxes of the SE and NW “starburst” components, but also a substantial contribution (30 to 50 percent) from the quasar warm dust component. The *Herschel* PACS fluxes at 160 and $70 \mu\text{m}$ (Leipski et al. 2010; rest frame 28 and $12 \mu\text{m}$) are entirely from the quasar-heated “warm” and “hot” dust components; the contributions from the SE and NW “starburst” components are negligible. The *Spitzer* MIPS flux at $24 \mu\text{m}$ (Hines et al. 2006; rest-frame $4.2 \mu\text{m}$) is mainly from the quasar-heated “hot” dust component. There is no contribution from the SE and NW “starburst” components.

4.6. Star-forming activity and merging

From the far-infrared luminosities derived above for the “cool”, “starburst” dust components, one can estimate the star formation rates following Kennicutt (1998):

$$\text{SFR} [M_{\odot}/\text{yr}] = 1.7 \times 10^{-10} L_{\text{FIR}} [L_{\odot}] \quad (4)$$

which yields 1000 and $2000 M_{\odot} \text{yr}^{-1}$ for the SE and NW components of BR1202-0725. The Kennicutt SFR relation is for a Salpeter Initial Mass Function (IMF). Adopting other IMFs, such as done by Kroupa (2001) or Chabrier (2005), would reduce these SFRs by about a factor of two. Even with a more top-heavy IMF however, it is clear that both the SE and NW galaxies have very intense starbursts, in multiple active regions. Depending on the IMF, the minimum times to consume all the molecular gas are 40 to 80 Myr (SE) and 30 to 60 Myr (NW), but longer if there are several, spaced-out, million-year bursts. These times are comparable to the ~ 40 Myr-consumption times in typical submm galaxies (SMGs) at $z \sim 2$ (Tacconi et al. 2008). The derived gas masses in BR1202-0725 are also about the same as in typical SMGs at $z \sim 2$. It is possible, that the quasar in the SE galaxy, and possibly a radio-quiet, dust-obscured AGN in the NW galaxy, contribute to the dust heating, and the star formation rate is overestimated. The other possibility is that we are observing an advanced multiple merger in BR1202-0725 close to the peak in its starburst luminosity curve, as shown by the wealth of components in the BR1202-0725 merger, including possibly two sources within each of the SE and NW galaxies, the active quasar, and the companion Lyman α protogalaxies. This wealth of activity may at least in part be a signature of the evolution of massive, high-redshift galaxies. Similar complexity will probably be discovered in the SMGs at $z \sim 2$, once they have been studied in comparable detail to BR1202-0725.

Rather than a merger of just two gas-rich galaxies, familiar from many ULIRGs at low redshift, the complexity of the BR1202-0725 interaction, with multiple galaxies or pre-galactic building blocks, may itself be a characteristic of the assembly of massive galaxies at high redshifts. Another high-redshift example of a complex merger is the $z = 3.8$ merger in the radio galaxy 4C41.17, where there are at least two CO sources, with a total CO(4–3) line width of 1000 km s^{-1} around the powerful AGN source of

the extended radio jets (De Breuck et al. 2005), as well as numerous near-IR companions (Graham et al. 1994), that appear like raisins in a pudding contracting to form a very massive galaxy. At least one of the companion regions, 4C41.17-South, has been shown to have the same redshift as the main AGN galaxy, 4C41.17-North (Van Breugel et al. 1999). Another relevant example is the $z=2.8$ multiple-galaxy merger in SMM J02399-0136 (see Ivison et al. 2010 and references therein), which also shows 1000 km s⁻¹-wide CO lines coming from the merger of a far-IR luminous but highly obscured starburst (their L2SW galaxy, coincident with a Ly α cloud), a BAL quasar host galaxy (their L1 galaxy) and two other components in the field (the L2 and L1NW galaxies). All four of these objects are at the same redshift (Ivison et al. 2010), and must be kinematically associated, not just seen in projection. As in BR1202-0725, the ensemble of merger components in SMM J02399-0136 form a vast and complex nursery, not only for new stars, but also for the formation of the future massive galaxy itself.

In the new data, the NW galaxy and the SE quasar host galaxy each break up into sub-components. Based on the present work, the BR1202–0725 group consists of at least four distinct sources (six when counting the faint Ly α companions). The proximity and similar redshifts of these galaxies or pre-galactic objects suggest that the SE quasar host galaxy, the obscured NW submm galaxy, and the Ly α objects are all in a gravitationally-bound group of galaxies that have decoupled from the cosmological expansion, and are probably merging together. All of these objects thus have exactly the same cosmological redshift, and the slight differences in their measured redshifts are due to true kinematic motions due to their mutual interaction within their "local group."

In the standard cosmology, a $z = 4.7$ galaxy is at a comoving (tape-measure) distance from us of 7.6 Gpc, and the lookback time is 12.4 Gy. When the galaxy emitted the light we now receive, its recession velocity was 2.3 c , the Hubble parameter, $H(z = 4.7)$ was 505 km s⁻¹ Mpc⁻¹, the only relevant component of the universe was matter, with $\Omega_M = 0.98$, and dark energy was irrelevant, with $\Omega_\Lambda = 0.014$ (see e.g., formulae in Ryden 2002; Liddle 2003). In the usual interpretation, the BR1202-0725 group is in the potential well of a overdensity of matter relative to the mean density of the universe, that, long before the $z = 4.7$ epoch, had decoupled from the cosmic expansion, so the galaxies in the group have only true kinematic relative motions governed by the total mass in the overdensity region. The greater neighborhood of the BR1202-0725 overdensity region as a whole may be similar to the numerous "redshift sheets" seen at high- z in the Hubble Deep Field (Cohen et al. 2000), or to the recently-found galaxy groups at $z = 5.2$ (Capak et al. 2011; Walter et al. 2012). In interpretations of the same-redshift groups, (e.g., Cohen, Hogg, & Blandford 2000, their sect. 6), these regions extend over several Mpc and have virial masses of a few times 10¹³ to 10¹⁴ M $_\odot$, resulting in true kinematic velocity dispersions (not cosmological redshifts) of a few hundred km s⁻¹. Our measured line-of-sight velocity differences of the different BR1202-0725 objects are of this order, and due to the close approaches (projected separations 3 to 25 kpc) in the individual mergers, the relative velocities can be even higher.

In other respects, the BR1202-0725 objects agree with the general picture of high-redshift protogalaxies.

Numerous deep-field morphological studies show that at high- z , there are no spirals (e.g., Driver et al. 1998; Abraham & van den Bergh 2002). The galaxies are gas-rich, puffed-up disks or spheroids, and much smaller than modern-day galaxies. The data of, e.g., Oesch et al. (2010) show that the half-light radii decrease as $(1+z)$ to the 1.1 to 1.3 power. At $z = 4.7$, typical galaxy radii are 700 to 1400 pc, depending on the mass. The high end of this range is close to sizes measured in the present paper for the BR1202-0725 SE and NW galaxies.

5. Conclusions

Our high-resolution millimeter observations of the BR1202-0725 galaxy complex at $z = 4.7$, in both line and continuum emission, reveal new aspects of this extreme multiple merger. Morphological and dynamical evidence together with the lack of any lens candidate or arc-like structure in the field, at any wavelength, definitely rule out the hypothesis that the obscured NW galaxy and the SE quasar host galaxy are lensed multiple images of the same background object. Instead, the present data indicate that the images of BR1202–0725 directly show a group of merging and very active starburst galaxies (Fig. 6, right).

The SE galaxy merger contains at least two sources. The main SE core source coincides with the optical quasar's position and shows internal kinematics compatible with rotation and a CO line profile (FWZP = 700 km/s) typical of a massive disk galaxy. To the southwest, the CO(5–4) line is narrower, with a linewidth of 200 km s⁻¹, and blueshifted by -180 km s⁻¹ relative to the main SE velocity peak. This fainter CO does not coincide in position with the weaker SW continuum source reported in the ALMA data (Wagg et al. 2012), which may be a third, fainter, galaxy in the merger.

The NW galaxy contains at least two sources, a main core source, and a fainter companion to the west/northwest at a velocity different by 600 km s⁻¹ from the main NW core. This second galaxy in the interaction accounts for the unusually broad total CO linewidth (FWZP > 1500 km/s) of the NW galaxy merger.

The far-IR luminosities of both sources are high, of order 10¹³ L $_\odot$, indicating tremendous star-forming activity, with estimated star formation rates greater than 1000 M $_\odot$ yr⁻¹. Since BR1202–0725 is radio quiet, its activity must be dominated by the massive starbursts that occur simultaneously in the galaxies interacting in the NW and SE components. We are obviously witnessing an extreme merging event in a group of galaxies, probably the youngest complex merger so far known. Future higher angular resolution observations of BR1202–0725 will allow us to better disentangle the properties of the individual starbursts that are interacting and merging, resulting in the remarkable appearance of this high-redshift object.

Acknowledgements. These observations were done with the IRAM Plateau de Bure Interferometer. IRAM is supported by INSU/CNRS (France), MPG (Germany) and IGN (Spain). The authors are grateful to the IRAM staff for their support. We thank Emmanuel Momjian for information on the VLBI positions, Juan Uson for useful comments, and the referee for very helpful criticism.

References

- Abraham, R.G., & van den Bergh, S. 2002, in *Disks of Galaxies: Kinematics, Dynamics, and Perturbations*, ed. E. Athanassoula, A. Bosma, ASP Conf. Ser. 275, 89
- Auger, M.W., Treu, T., Bolton, A.S., Gavazzi, R., et al. 2010, ApJ, 724, 511
- Benford, D.J., Cox, P., Omont, A., Phillips, T.G., & McMahon, R.G. 1999, ApJ, 518, L65
- Bothwell, M.S., Smail, I., Chapman, S.C., et al. 2012, MNRAS, in press, arXiv:1205.1511
- Broadhurst, T., & Lehar, J. 1995, ApJ, 450, L41
- Carilli, C., Kohno, K., Kawabe, R., Ohta, K., et al. 2002, AJ, 123, 1838
- Capak, P., Riechers, D., Scoville, N.Z., et al. 2011, Nature, 470, 233
- Chabrier, G., 2005, in *The Initial Mass Function 50 Years Later*, ed. E. Corbelli, F. Palla, & H. Zinnecker, (Dordrecht: Springer), p. 41
- Cohen, J.G., Hogg, D.W., Blandford, R., et al. 2000, ApJ, 538, 29
- De Breuck, C., Downes, D., Neri, R., van Breugel, W., Reuland, M., Omont, A., & Ivison, R. 2005, A&A, 430, L1
- Djorgovski, S., & Davis, M. 1987, ApJ, 313, 59
- Downes, D., & Solomon, P. 1998, AJ, 507, 615
- Driver, S.P., Fernandez-Soto, A., Couch, W.J., et al. 1998, ApJ, 496, L93
- Egami, E., Neugebauer, G., Soifer, B.T., et al. 2000, ApJ, 535, 561
- Eisenhardt, P.R., Armus, L., Hogg, D.W., Soifer, B.T., Neugebauer, G., & Werner, M. 1996, ApJ, 461, 72
- Evans, I.N., et al. 2010, ApJS, 189, 37
- Faber, S.M., Dressler, A., Davies, R.L., Burstein, D., & Lynden-Bell, D. 1997, in “Nearly Normal Galaxies”, ed. S.M. Faber, (New York: Springer), p. 175
- Feruglio, C., Fiore, F., Maiolino, R., et al. 2012, A&A, in press.
- Fontana, A., Cristiani, S., D’Odorico, S., Giallongo, E., & Savaglio, S. 1996, MNRAS, 279, L27
- Fontana, A., D’Odorico, S., Giallongo, E., Cristiani, S., Egami, E., Hu, E., & McMahon, R.G. 1997, in *Dust and Visible Matter in Galaxies*, ed. M. Persic & P. Salucci, ASP Conf. Ser., 117, 477
- Fontana, A., D’Odorico, S., Giallongo, E., Cristiani, S., Monnet, G., & Petitjean, P. 1998, AJ, 115, 1225
- Fontana, A., D’Odorico, S., Poli, F., et al. 2000, AJ, 120, 2206
- Giallongo, E., D’Odorico, S., Fontana, A., Cristiani, S., Egami, E., Hu, E., & McMahon, R.G. 1998, AJ, 115, 2169
- Graham, J.R., Matthews, K., Soifer, B.T., et al. 1994, ApJ, 420, L5
- Guilloteau, S. 2001, in *Science with the ALMA*, ed. A. Wooten (San Francisco: ASP) ASP Conference Series 235, 271,
- Hines, D.C., Krause, O., Rieke, G.H., Fan, X., Blaylock, M., & Neugebauer, G. 2006, ApJ, 641, L85
- Hogg, D.W., Cohen, J.G., & Blandford, R. 2000, ApJ, 545, 32
- Hu, E.M., McMahon, R.G., & Egami, E. 1996, ApJ, 459, L53
- Hu, E.M., McMahon, R.G., & Egami, E. 1997, in *The Hubble Space Telescope and the High-Redshift Universe*, ed. N.R. Tanvir, A. Aragon-Salamanca, J.V. Wall, (Singapore: World Scientific), p. 91
- Hughes, D.H., Dunlop, J.S., & Rawlings, S. 1997, MNRAS, 289, 766
- Iono, D., Yun, M.S., Elvis, M., Peck, A.B., Ho, P.T.P., Wilner, D.J., Hunter, T.R., Matsushita, S., & Muller, S. 2006, ApJ, 645, L97
- Ivison, R.J., Smail, I., Papadopoulos, P.P., et al. 2010, MNRAS, 404, 198
- Kennicutt, R.C. 1998, ApJ, 498, 541
- Komatsu, E. et al. 2011, ApJS, 192, 17
- Kroupa, P. 2001, MNRAS, 322, 231
- Krügel, E., & Siebenmorgen, R. 1994, A&A, 288, 929
- Leipski, C., Meisenheimer, Klaas, U., et al. 2010, A&A, 518, L34
- Liddle, A., 2003, *An Introduction to Modern Cosmology*, Wiley
- McMahon, R.G., Omont, A., Bergeron, J., Kreysa, E., & Haslam, C.G.T. 1994, MNRAS, 267, L9
- Momjian, E., Carilli, C., & Petric, A. 2005, AJ, 129, 1809
- Oesch, P.A., Bouwens, R.J., Carollo, C.M., et al. 2010, ApJ, 709, L21
- Ohta, K., Yamada, T., Nakanishi, K., Kohno, K., Akiyama, M., Kawabe, R. 1996, Nature, 382, 426
- Ohyama, Y., Taniguchi, Y., & Shioya, Y. 2004, AJ, 128, 2704
- Omont, A., Petitjean, P., Guilloteau, S., et al. 1996, Nature, 382, 428
- Ossenkopf, V., & Henning, T. 1994, A&A, 291, 943
- Petitjean, P., Pécontal, E., Valls-Gabaud, D., & Charlot, S. 1996, Nature, 380, 411
- Riechers, D.A., Walter, F., Carilli, C.L., et al. 2006, ApJ, 650, 604
- Ryden, B., 2002, *Introduction to Cosmology*, Addison-Wesley
- Sanders, D.B., Scoville, N.Z., & Soifer, B.T. 1991, ApJ, 370, 158
- Sluse, D., Schmidt, R., Courbin, F., et al. 2011, A&A, 528, 100
- Solomon, P.M., Rivolo, A.R., Barrett, J., & Yahil, A. 1987, ApJ, 319, 730
- Solomon, P.M., Downes, D., & Radford S, 1992, ApJ, 398, L29
- Tacconi, L.J., Genzel, R., Smail, I., et al. 2008, ApJ, 680, 246
- Trentham, N. 1995, MNRAS, 277, 616
- Van Breugel, W., Stanford, A., Dey, A., et al. in *The Most Distant Radio Galaxies*, ed. H.J.A. Röttgering, P.N. Best, & M.D. Lehnert (Roy. Neth. Acad. Sci.: Amsterdam), 49
- Van der Tak, F.F.S., Black, J.H., Schöier, F.L., Jansen, D.J., van Dishoeck, E.F. 2007, A&A 468, 627
- Venemans, B.P., McMahon, R.G., Walter, F., et al. 2012, ApJ, 751, L25
- Wagg, J., Wiklind, T., Carilli, C.L. et al. 2012, ApJ, 752, L30
- Walter, F., Decarli, R., Carilli, C., et al. 2012, Nature, 486, 233
- Weiss, A., Henkel, C., Downes, D., & Walter, F. 2003, A&A, 409, L41
- Weiss, A., Downes, D., Henkel, C., & Walter, F. 2005, A&A, 429, L25
- Weiss, A., Downes, D., Neri, R., Walter, F., Wilner, D.J., Wagg, J., & Wiklind, T. 2007, A&A, 467, 995
- Wright, E.L. 2006, PASP, 118, 1711

Appendix A: Absence of gravitational lensing

Whether the submm/radio companion is a distinct object or a gravitational image of the quasar host galaxy is an important question because in the absence of magnification, BR1202–0725 would be the most luminous binary CO and far-IR source in the Universe. The observational facts do indeed speak against gravitational lensing. The difference in linewidths of the NW and SE sources, the absence of optical or UV emission from the NW source, and the multiple CO and dust components in each source, are all difficult to reconcile with a gravitational lensing scenario to account for the appearance of BR1202–0725. In the following discussion of gravitational lensing, we definitely rule out the hypothesis that the SE and NW sources are multiple lensed images of the same background source.

A.1. Different linewidths.

The main piece of evidence comes from the greatly different molecular and atomic emission line profiles observed towards the NW and SE sources. These NW and SE CO and carbon-line profiles are so different in their widths and peak velocities, that they cannot be gravitational images of a single object. Differences in velocities and linewidths might occur in multiple lensed images of optical lines, if, for example, a multiply-imaged quasar were locally magnified by a micro-lensing event that would affect only one of the images. Such an effect cannot affect the submm CO and carbon lines, however, because these low brightness, high luminosity lines are emitted over a large (≥ 2 -kpc), relatively cool (50 to 100K) region, and unlike the small, hot, accretion disk of a quasar, cannot be affected by micro-lensing. Differential image magnification between the NW and SE CO sources can also be ruled out; although the SE and NW CO sources have quite different linewidths, their dust continuum fluxes are nearly the same. The dust sources and the molecular line sources are observed at the same wavelengths, and their measured sizes ($\sim 0.5''$) are roughly the same, so there is no evidence for any differential magnification between the SE and NW sources at submm wavelengths.

A.2. No optical counterpart of the NW galaxy.

The second piece of evidence comes from the dissimilarity of the optical and mm/submm images of the quasar and its main companion, the NW source. The SE submm dust and molecule component is associated with an optically-bright quasar whose light is not seen at the position of the NW submm component. The nearly unsurmountable problem is to make a gravitational lensing model that would produce a single-spot optical image and a double-spot submm image. To first order, gravitational lensing is achromatic *if the source size is the same at different wavelengths*.

But the quasar optical light (rest-frame UV) and its broad lines come from the black hole accretion disk on a scale of 10^{-2} pc, while the low-brightness-temperature CO lines and submm dust emission must be of kpc-scale size to be detectable at all at high redshifts. The molecular disk area is thus 10^{10} times larger than the quasar accretion disk area, and this can lead to dramatic differences in lensing amplification and lensed image shapes between optical and submm wavelengths.

Two examples are IRAS F10214+4724, and APM 08279+5255. In F10214, the quasar is too obscured to be visible, but the AGN optical narrow-line region is magnified by a factor of 100, while the much larger submm molecular disk is magnified by only a factor of 10. (see models by Broadhurst & Lehar 1995; Trentham 1995; Eisenhardt et al. 1996). In APM 08279, the quasar’s rest-frame UV through mid-IR is also magnified by factor of 100, while the cold part of the submm molecular disk is magnified by much less (see model by Egami et al. 2000, their Fig. 9). But even in these models with large differences in magnification between the optical and submm, it is nearly impossible to simultaneously produce a double image at submm wavelengths, and only a single image at optical wavelengths.

In a lensing scenario, one would have to imagine a galaxy on the line of sight somehow producing a double image only of the molecular disk, but not of the optical quasar, and then, in addition to this first lens that images only the molecular disk, a second lens producing a strong micro-lensing of the quasar to make an optically bright, single, quasar image, with no micro-lensing amplification of the much larger molecular disk. This overly-complicated scenario would not work at near-IR wavelengths of 3.6 and $4.6\mu\text{m}$, (rest wavelengths 6300 and 8070\AA), however, because the emitting region, the hot outer parts of the circumnuclear ring around the quasar, are large compared to a typical micro-lensing Einstein radius (e.g., Sluse et al. 2011).

Contradicting this scheme, the *Spitzer* archive images at 3.6 and $4.6\mu\text{m}$ show that the quasar is indeed much brighter (>100 times) than any object toward the NW, in the near-IR. In fact, the light that is seen in the NW in *Spitzer* data is actually the extended starlight continuum from the Ly α 1 companion galaxy, which is also near-IR bright in the *R*, *I*, and *K* bands (see discussion of their *Spitzer* data by Hines et al. 2006). The submm dust and molecular disks in the SE and NW galaxies that are discussed in the present paper cannot be detected in the *Spitzer* near-IR images, because they are too cold; their flux is hopelessly far down the Wien side of the blackbody curve, and they do not radiate at all at rest-frame optical wavelengths (Fig. 8).

All these difficulties to find a lensing model that would produce a single-spot optical quasar image and a double-

spot submm image, such as a galaxy-mass lens for a double-image molecular disk only, simultaneously with stellar-mass micro-lensing for the quasar only, that doesn’t really work for the near-IR images, lead us to conclude that a lensing explanation is a blind alley.

A.3. Absence of a candidate deflector to make a double image.

Deep optical images from the *HST* and VLT do not show any evidence of a massive foreground object capable of deflecting the light of the quasar of BR1202–0725 into two widely-separated images. Nor do they show any evidence of any arc-like structure, neither on galaxy-lensing angular scales, nor on cluster-lensing angular scales.

Because the SE and NW sources have similar fluxes in the submm continuum and in the CO, [CI], and [CII] emission lines, the most natural hypothesis for gravitational lensing would be a fairly circularly symmetric mass distribution located close to the mid-point of the $4''$ line connecting the two sources. Deep ESO-NTT imaging (Fontana et al. 2000) of the system along with *BVRIK* data (Giallongo et al. 1998) allow us to put tight upper limits on the deflector brightness.

To produce an image splitting of $\Delta\theta = 4''$, a deflector at redshift z_L , that for simplicity we approximate as a Singular Isothermal Sphere, would need to have a velocity dispersion given by:

$$\sigma = 186.25 \text{ km/s} \cdot \sqrt{\frac{\Delta\theta}{2w}}, \quad (\text{A.1})$$

where $w = d_{LS}/d_S$ is the ratio of the angular diameter distances between the deflector and the source and between the observer and the source. We get a sensible value of $\sigma \lesssim 350 \text{ km s}^{-1}$ only if $z_{\text{lens}} \lesssim 1$. Furthermore, from the Faber-Jackson relation (e.g., Faber et al. 1987; Djorgovski & Davis 1987), one can estimate the rest-frame luminosity of such a deflector and, for a SED typical of a massive galaxy, one can predict the redshifted *r*-band magnitude. For any redshift $z_{\text{lens}} \lesssim 1$, the deflector would have a magnitude ≤ 24 and be bright enough to be detectable in the *HST* image. We thus conclude that, unless the deflector is very atypical relative to more local lensing galaxies (e.g., Auger et al. 2010), one would be able to detect it.

The brightest near-IR object in the vicinity of BR1202–0725 is the faint Ly α 1 companion galaxy located between the NW and SE sources, which has an *r* magnitude of 24.3. It cannot play the role of a deflector, as it has the same redshift as BR1202–0725 and is much too faint. The second, even fainter, Ly α 2 companion galaxy lies $3''$ southwest of BR1202–0725, but it is again at the same redshift as the quasar (Hu et al. 1996; 1997).

Finally, there is no arc-like feature on deep optical images that would indicate very strong magnification of the bright quasar. Such an arc-like feature might arise if the quasar (only) were on the infinite-magnification caustic of a lens so close to the line of sight to the quasar itself, that the lensing galaxy would be visible neither against the quasar light, nor even on images where the quasar light is subtracted out, such as the quasar-subtracted images of Fontana et al. (1996) and Hu et al. (1996).

In summary, there is no evidence, at any wavelength, for a galaxy-mass lens along the line of sight to BR1202–0725, that could produce a submm double image.

A.4. Absence of a nearby cluster lens for overall magnification

Apart from trying to explain the submm double source by lensing by a galaxy-mass deflector, one might ask whether the entire BR1202-0725 complex could be lensed by foreground cluster of galaxies. In this case, the NW and SE submm sources are indeed independent galaxies, but each of them, and the optical quasar, might be amplified by a comparable amount, by a large, low-redshift foreground lens, i.e., a cluster of galaxies. Here, the answer is no. The BR1202-0725 region has been the object of a deep-field survey, the NTT BR1202 field, together with an overlapping region, the NTT Deep Field, resulting in a total field of $2.3' \times 4'$ (Fontana et al. 2000). These two overlapping deep fields were surveyed in $UBVr$ bands and in the near-IR IJK bands. Magnitude limits were of order 26 in r and 21.7 in K . Although there is a peak in the redshift distribution at $z \sim 0.6$ (Giallongo et al. 1998), there is no evidence for a cluster of galaxies that could act as an overall magnifier for the BR1202-0725 complex as a whole. Nor is there any systematic lengthening of galaxy images into ellipses or arcs that would be signatures of large-scale magnification across the field.